IEEE Access
Multidisciplinary | Rapid Review | Open Access Journal

Received February 28, 2021, accepted March 30, 2021, date of publication April 2, 2021, date of current version April 13, 2021.

Digital Object Identifier 10.1109/ACCESS.2021.3070531

Post-Fault Demagnetization of a PMSG Under Field Oriented Control Operation

ROBERTO EDUARDO QUINTAL-PALOMO[1], (Member, IEEE), MANUEL FLOTA-BAÑUELOS[1], (Member, IEEE), ALI BASSAM[1], RICARDO PEÓN-ESCALANTE[1], FRANCISCO PEÑUÑURI[1], AND MATEUSZ DYBKOWSKI[2]

[1]Faculty of Engineering, Universidad Autónoma de Yucatán, Merida 97000, Mexico
[2]Department of Electrical Machines, Drives and Measurements, Wrocław University of Science and Technology, 50-370 Wrocław, Poland

Corresponding author: Roberto Eduardo Quintal-Palomo (roberto.quintal@correo.uady.mx)

This work was supported in part by the Mexican Council of Science and Technology (CONACYT) under Grant 312140.

ABSTRACT To assess demagnetization, a line-to-line short-circuit fault study is carried out with constant input torque and field-oriented control (FOC) for the speed of a permanent magnet synchronous generator (PMSG). For the study, a cosimulation between finite element analysis (FEA), power electronics simulation (Simplorer) and model-based control design software (Matlab Simulink) is used. The analyzed system was previously validated in the experimental set-up with DS1103 card. The initial short circuit currents, although higher than nominal, did not present a risk of demagnetization for the generator in the analyzed working conditions, namely magnets temperature and speed. Nevertheless, the acceleration during the fault, due to constant input torque, and the control scheme with a constant speed reference, provided a greater demagnetizing current while breaking the machine speed back to the pre-fault reference. The cosimulation results bring higher fidelity to the modeling and analysis of the behavior of the PMSG under FOC.

INDEX TERMS Demagnetization, fault tolerance, finite element analysis, machine vector control, permanent magnet machines, space vector pulse width modulation.

I. INTRODUCTION

Permanent magnet synchronous machines (PMSM) have been gaining importance in the last two decades due to the advancements in material science related to the maximum energy density ($BH_{\max}$) of hard magnetic materials [1], this characteristics allowed the machines to have higher efficiencies and to be more compact [2]. On the other hand, rare earth magnets with the highest energy density, neodymium magnets (Nd-Fe-B), also have temperature dependent magnetization curves with knee points at lower coercivity than other materials, see Fig. 1, this means that Nd-Fe-B magnets can suffer irreversible demagnetization or partial demagnetization at temperatures higher than 80°C.

Early attempts to include such demagnetization effects in the analysis of electrical machines can be found in [3]–[6]. In [7] Fu demonstrated an algorithm to implement the nonlinear characteristic using only the normal *B-H* curve as an input of the time-stepping field-circuit coupled Finite Element Analysis (FEA), this was done with a dynamic computation of the *B-H* curve for each operating point. In [8] the first temperature-dependent demagnetization model was implemented inside a commercial FEA software ANSYS Maxwell. Some years before, the same company had implemented the link between the field-circuit coupled time stepping simulation and a multidomain simulation software (Simplorer) for modeling of the power electronics interaction with the electrical machine as shown in [9].

Some early results published with the FEA demagnetization model can be found in [10]–[12]. In the last decade the use of transient FEA has been widely adopted for demagnetization studies, partially thanks to the close agreement of the FEA results with experiments. For example, in [13] a samarium cobalt magnet was demagnetized in an experimental fixture which was also modeled in FEA software COMSOL, with good agreement between FEA results and measurements. A similar experiment was carried out for a Nd-Fe-B magnet, where, also a strong demagnetizing magneto motive force was applied, both in FEA software JMAG and in the experiment. Recently, a similar experiment was

The associate editor coordinating the review of this manuscript and approving it for publication was Heng Wang.

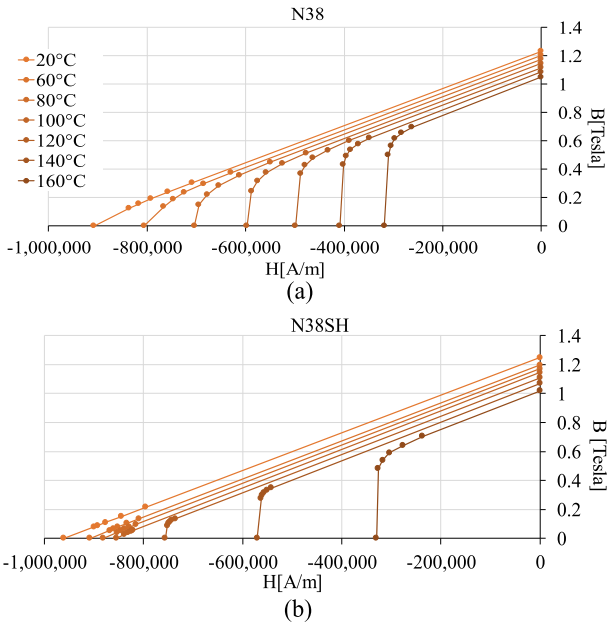

FIGURE 1. Nd-Fe-B magnet temperature dependent nonlinear B-H curve magnetization characteristic (a) and with added dysprosium (b).

done by the same authors in [14], but this time the temperature dependency of the magnetization was tested both experimentally and with 3D FEA presenting very similar demagnetization results, as measured over the magnet.

Specifically, for the PMSM rotor demagnetization, the studies done by Hur in [15] analyzed a 6 pole interior permanent magnet (IPM) motor with inter-turn short circuit fault at 150°C inside a temperature chamber, and compared his measurements with 2D FEA results. Again, Hur in [16] revisited the experiment adding a surface permanent magnet rotor and a dynamic analysis, namely time-stepping FEA, obtaining even more similar results to measurements.

Other authors have also done complete IPM motor demagnetization tests like Jahns in [17] first in FEA only, and then experimentally in [18], without a temperature chamber but rather with a heat gun pointing at the rotor magnets. It is important to mention previous work by Welchko *et al.* [19] and Choi and Jahns [20],[21] that has also focused on the effect of 3-phase short-circuit faults (symmetrical short-circuit) and line-to-line short-circuit faults (asymmetrical short-circuit), leading to the conclusion that the asymmetrical short-circuit is the most dangerous for demagnetization of IPM motors in [20].

In this work, to achieve demagnetization, an asymmetrical line-to-line short-circuit fault is applied to a permanent magnet synchronous generator (PMSG) under constant input torque from the prime mover, and constant speed control.

In order to assess the overall effect of demagnetization in the complete system, a cosimulation was done, namely a FEA linked with Simplorer for power electronics, and to Matlab Simulink, a software extensively used in automatic control for model-based design, this is as shown in Fig. 2.

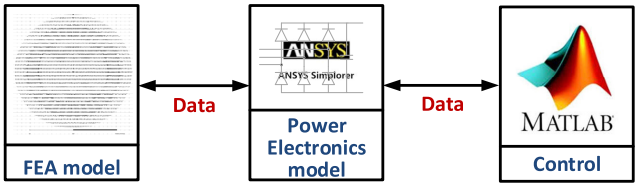

FIGURE 2. The cosimulation approach.

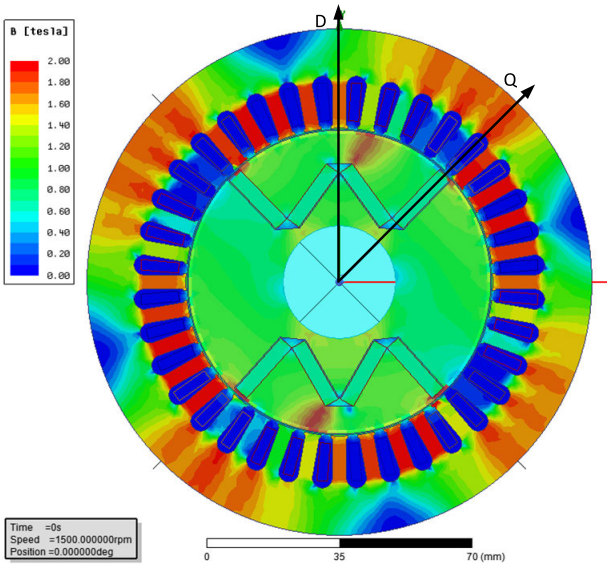

FIGURE 3. Magnetic field density B and DQ vectors over the geometry of the PMSG.

In section II the PMSG is presented and its main characteristics explained as well as some open loop measurements done in order to validate the FEA model, in section III the control scheme is presented with some laboratory measurements made with a 2-level voltage source converter (VSC) under the field oriented control (FOC) scheme. Section IV presents the cosimulation layout and the results of the cosimulation with the asymmetrical short-circuit. Finally, section V presents the conclusions of the obtained results.

II. MODEL OF THE CONSEQUENT POLE PMSG

The PMSG studied, is an asymmetric IPM with 4 poles, two of which are ''consequent poles'' as named in the literature [22], sometimes referred as ''induced poles'' e.g. in [23]. This configuration is preferred because it uses half the number of magnets than the traditional 4 pole IPM rotors. In Fig. 3 the magnetic flux density B of the generator is presented. Notice the W shape position of the magnets. Also notice that the upper W is not identical to the lower one. This was done in order to obtain asymmetrical poles. A detailed explanation of the design process and optimization of the W shape was published in [24].

The design of the PMSG was based on the series-produced three-phase induction motor, the Sh90-L4 [25]. Housing, stator, and shaft are the same, but the rotor was designed to accommodate 4 poles made from 18 by 4 by 30 mm rectangular cuboid N38SH Nd-Fe-B magnets. The SH rating

TABLE 1. Characteristics of the PMSG.

Phases	3
Connection	star
Nominal power	2.2 kW
Nominal speed	1500 rpm
Nominal frequency	50 Hz
Nominal current	3.5 A_{rms}
Nominal torque	15 N·m
Number of poles	4
Stator slots	36
Shaft diameter	30 mm
Efficiency measured at nominal speed and nominal torque	89%

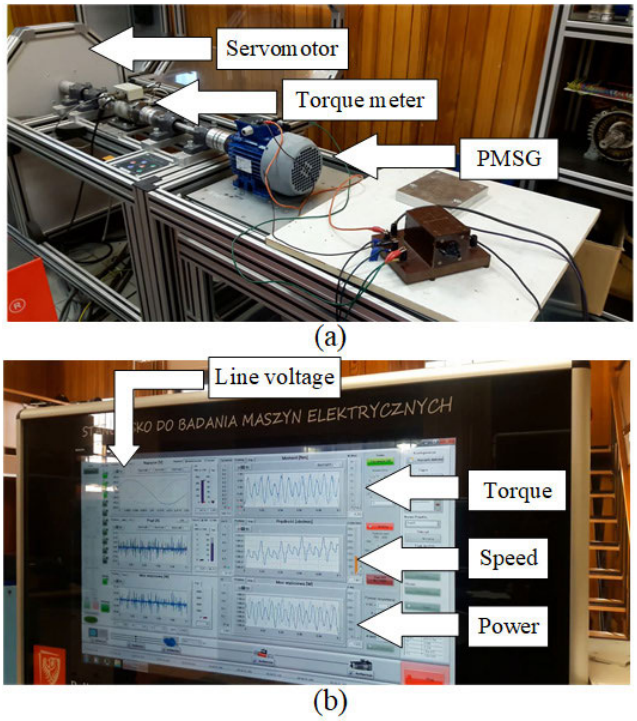

FIGURE 4. Laboratory bench for the open loop machine test (a) and the user interface for the measurements (b).

of the magnets refers to a suggested maximum operating temperature of 150°C as stated in [26]. This is by virtue of dysprosium (Dy) in the material powder content, which makes the magnet more resistant to demagnetization but at the same time more expensive, since Dy is even more expensive than neodymium. This is why is preferred to work with magnets with less content of Dy, but at the same time the possible demagnetization conditions need to be averted.

In Table 1 the main characteristics of the PMSG are presented. Notice that, although the Sh90-L4 induction motor efficiency is in the IE1 category (<80%), the PMSG obtains efficiencies around 90%, and higher output power thanks to the Nd-Fe-B magnets.

In Fig. 4 the laboratory test stand for the validation of the FEA model is presented. In this test bench, the PMSG was tested in open loop (no converter) to obtain the open circuit back EMF, and with a 3-phase resistor load.

In Fig. 5 and Fig. 6 some test results at different speeds with a purely resistive load are compared against FEA results.

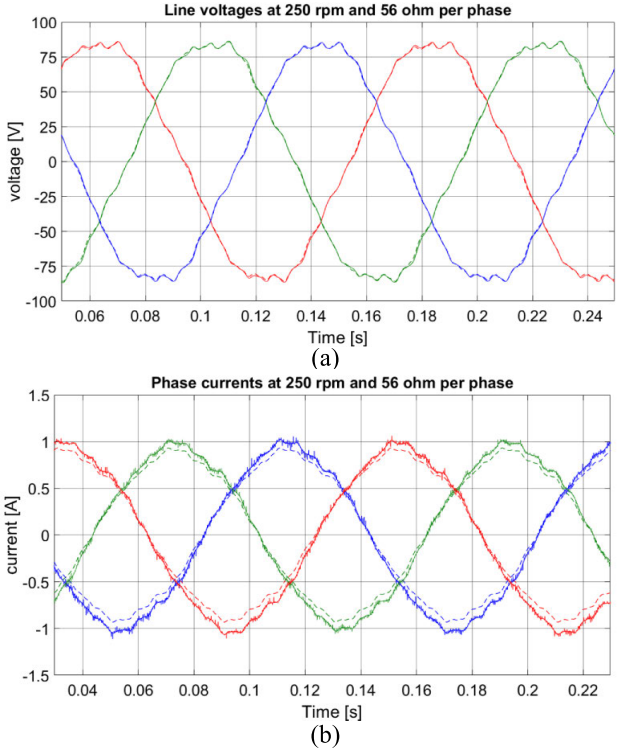

FIGURE 5. Comparison of measurements (solid line) and FEA results (dashed line) at 250 r/min, line voltages (a) and phase currents (b).

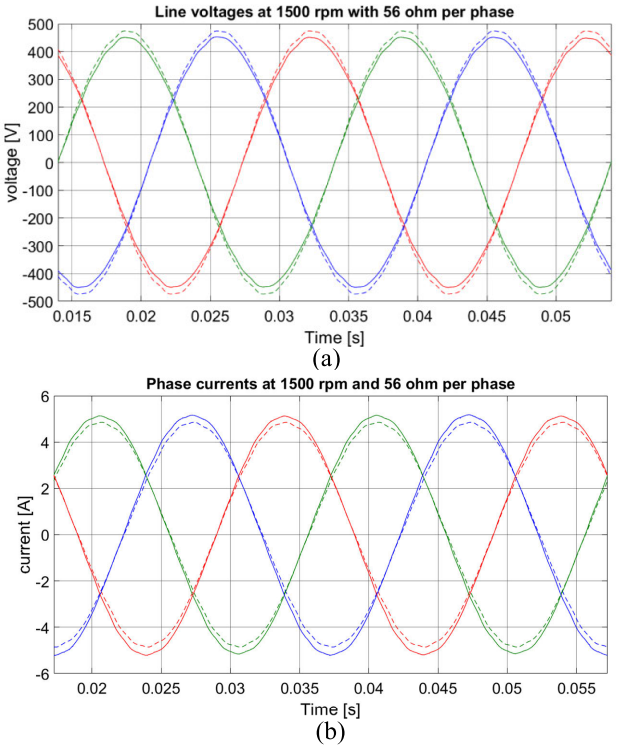

FIGURE 6. Comparison of measurements (solid line) and FEA results (dashed line) at 1500 r/min, line voltages (a) and phase currents (b).

Notice the similarities even in the shape of voltages and currents. Many tests were made at different speeds and different load values. All of them gave measurements within 5% of the FEA predicted results.

It is important to mention that the transient FEA results provide very similar waveforms to the measurements even with nonlinear components connected (e.g. diodes), this was proven and published by one of the authors in [27]. The results presented here and in the aforementioned literature make the cosimulation approach a very useful tool to assess the system behavior under operating conditions difficult to replicate in the laboratory.

III. FIELD ORIENTED CONTROL

In Fig. 7 the control scheme for the speed of the PMSG is presented. Notice that the reference for $I_{\mathrm{d,ref}}$ current is zero.

In order to test this control scheme with the PMSG, the machine was installed in another test bench with an induction motor as the prime mover, see Fig. 8.

An IGBT based voltage source converter connected to the PMSG and to a rapid control prototyping board, a DS1103 and its host computer was used.

In Fig. 9 some results obtained from this setup are presented. Before 1 s, the prime mover start spinning the PMSG close to nominal speed in open loop. It is important to observe

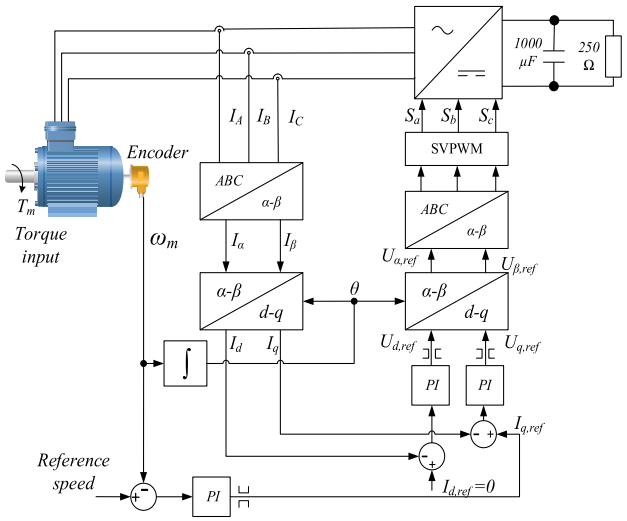

FIGURE 7. Control scheme of the PMSG to maintain a reference speed.

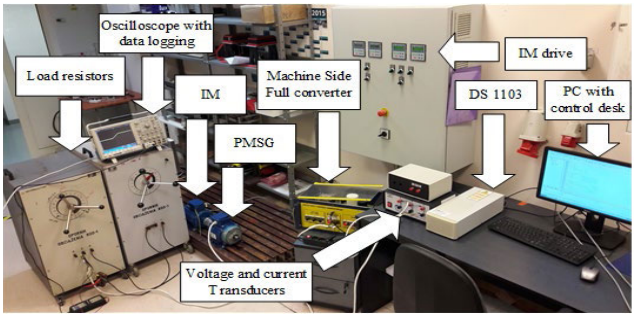

FIGURE 8. Test bench for the closed loop control system.

in Fig. 9a the system response when the converter is turned on. This is also noticeable in Fig. 9c since the phase currents are more sinusoidal.

In Fig. 9b, notice the shape of the currents due to the freewheeling diodes of the IGBTs that act as full wave rectifier. This shape of the currents is similar to the ones obtained under similar conditions with a full wave rectifier, in measurements and FEA as in Fig. 10 and in [27].

Further analyses were done in this setup, although is important to mention that the induction motor used as prime mover had a lower power rating (torque) than the PMSG. Due to this situation only 7 N · m input torque were available to spin the PMSG.

In Fig. 11 the DC bus voltage and angular speed of the same experiment shown in Fig. 9. Notice that the angular speed has a very long sag. This is because the lower power rating of the IM used as a prime mover.

In Fig. 12 the comparison between the phase current measurements under FOC and FEA cosimulation results. Notice that FEA results look more distorted. This may be because the measurements include additional inductance from cables and contact resistance from terminals. Also, the effect of the IGBTs switching is more visible in the cosimulation because the cables and transducers in the measurements may act as a low pass filter. In both, experiment and cosimulation the switching frequency was 3 kHz.

Another important comparison between measurements and FEA cosimulation is shown in Fig. 13.

The DQ currents in the rotating reference frame are compared with the ones calculated in the cosimulation. The FEA results look more distorted than the measurements because they are calculated from the same phase currents shown in Fig. 12 and the angular position θ.

IV. COSIMULATION

A. EXPERIMENT SETUP

As described in the introduction the main purpose of this work is to assess demagnetization risks of the PMSG. One of the mechanisms of demagnetization is shown in Fig. 14 where the stator currents, namely the armature reaction, drive the operating point below the knee point of the *B-H* curve. Once the operating point is in *B*, it will not come back to the previous operating point *A* but to *C* instead, rendering the magnet partially demagnetized.

As mentioned earlier, this material property has been included recently in the FEA software. The *B-H* curve of the N38SH magnet is given as input to the FEA. In this work, the magnet temperature was kept constant throughout the experiment at 100 °C. This is mainly because the temperature-change process, inside the spinning rotor, is considered to take longer time than the duration of the experiment.

In Fig. 15 the cosimulation setup of the experiment is shown. Notice the linking-blocks to the 2D FEA model and the Matlab Simulink. The machine is modeled in 2D finite element with 7644 elements. The IGBT converter is modeled

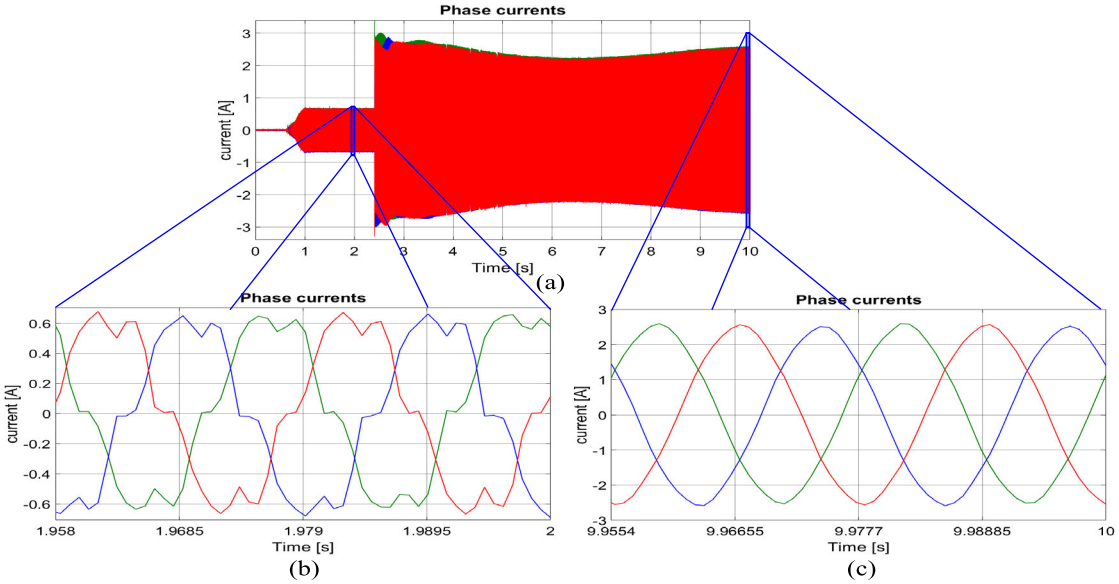

FIGURE 9. Measurements from the closed loop system. First the prime mover spins the machine and at 2.4 s the converter is turned on.

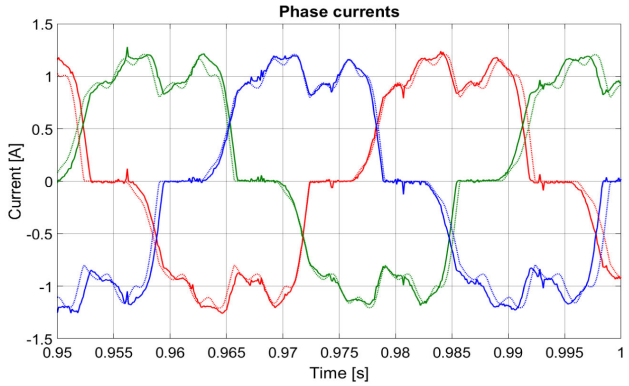

FIGURE 10. Comparison of current measurements (solid line) and FEA results (dotted line) for a full wave rectifier with a 240 Ω DC bus load.

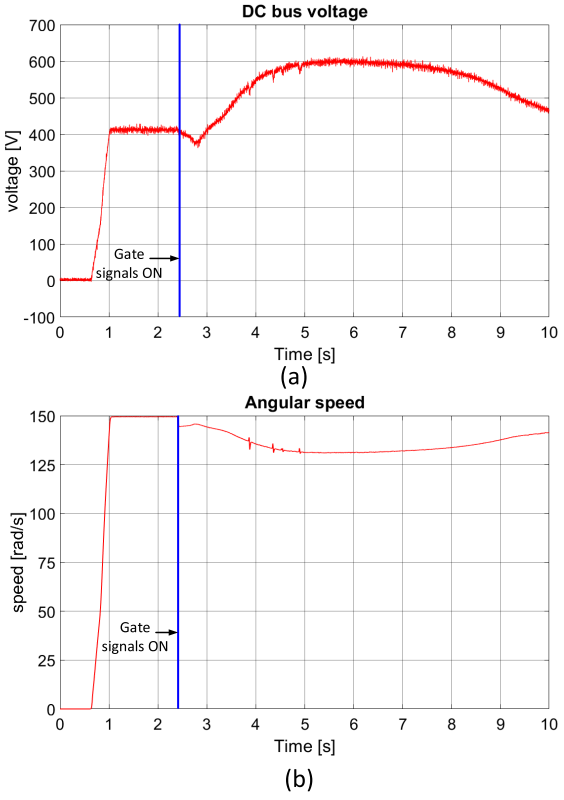

FIGURE 11. Measurements of DC bus voltage (a) and angular speed (b).

in the multidomain mixed signal simulator Simplorer and the control loop is running in Matlab Simulink. The Simplorer minimum time step (H_{min}) is 50μs. The Matlab Simulink control loop was solved by the "Trapezoidal rule + Backward differentiation formula" (ode23tb). As in the validations shown earlier, the space vector pulse width modulation has a 3 kHz frequency.

In Fig. 16 the input signals of the experiment are presented. Initially the prime mover ramps up to 15 N · m and stays constant throughout the whole experiment. Also, the reference speed signal initially ramps up to 157 rad/s (1500 r/min) and also stays constant.

The line-to-line short circuit occurs at 3 s and has a duration of 150 ms (<8 cycles). This was chosen to comply with the standard for bigger generators e.g. IEC/IEEE 62271-37-013. After 150 ms the fault is cleared but the reference speed and input torque stay constant.

B. RESULTS

In Fig. 17 the phase currents and angular speed feedback before, during and after the asymmetrical short-circuit are presented. In Fig. 17a notice that the peak current is reached after the short-circuit clearance. In Fig 17b notice that the

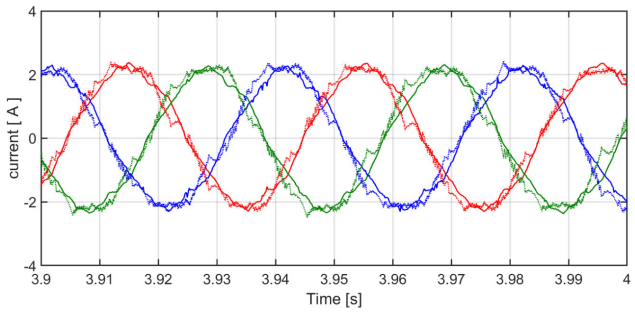

FIGURE 12. Comparison of current measurements (solid line) and FEA results (dotted line) for closed loop VSC controlled.

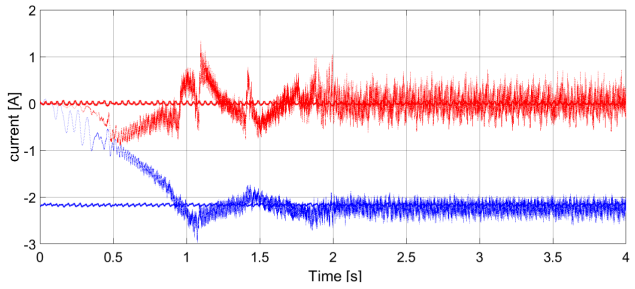

FIGURE 13. Comparison of DQ currents (red D, blue Q) measurements (solid line) and FEA results (dotted line) for closed loop with VSC.

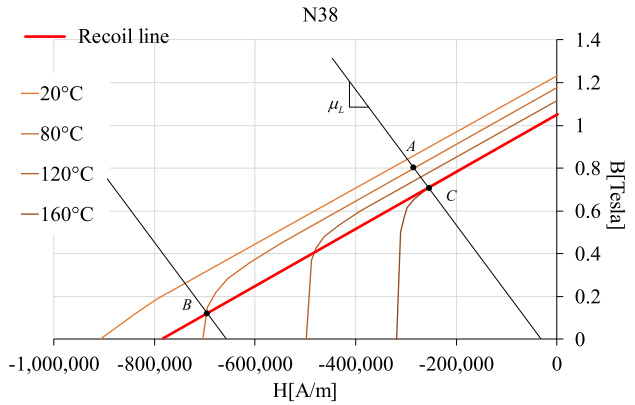

FIGURE 14. Recoil line of the Nd-Fe-B magnets.

machine accelerates during the short-circuit, and then decelerates after the short circuit is cleared. It is important to note that the peak currents in Fig. 17a are coincident with the sudden deceleration in Fig. 17b, at about 3.65 s.

In Fig. 18 a close-up of the phase currents during the short-circuit, and after the short circuit clearance is presented. Notice that the short-circuit currents are higher than the ones at nominal conditions, namely 1500 r/min and 15 N·m input torque. Even though the asymmetrical short-circuit currents go up to 15 A_{peak} for this machine, the peak currents reached after the fault clearance are clearly larger, up to 40 A_{peak}.

In Fig. 19 the DQ currents and the DQ outputs of the FOC system are presented. Notice that the D currents turn

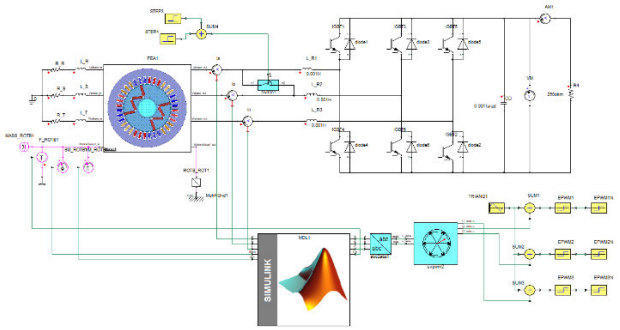

FIGURE 15. Setup of the cosimulation experiment with line-to-line switch.

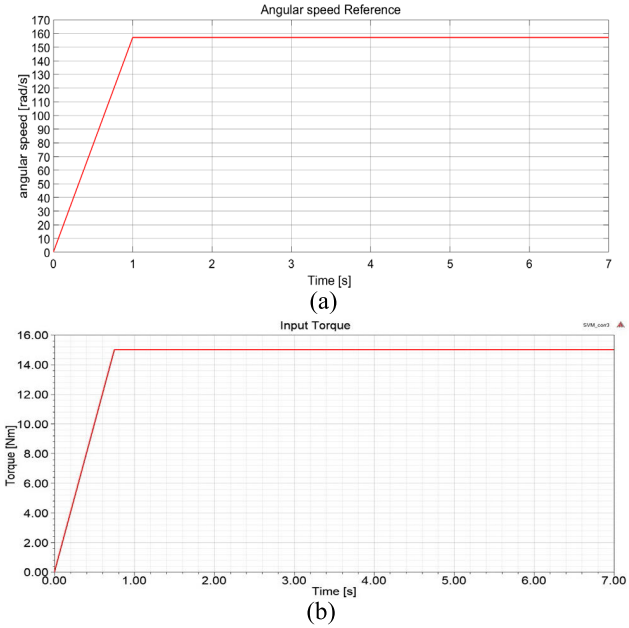

FIGURE 16. Angular speed reference input (a) and input torque (b).

into negative values immediately during the short-circuit and stay negative after the short-circuit clearance. Once again, the peak value of the D current occurs after the fault, reaching ∼24 A in the negative D direction.

Having a negative D current means that the PMSG is at higher risk of demagnetization because this current is generating a magnetic field in the direction opposing the magnets, therefore shifting the operating points closer or even below the knee point of the *B-H* curve.

In Fig. 19b the current controller output of the FOC is shown. Bear in mind that the input torque and speed reference are constant before and after the fault. This means that the difference at steady state of these signals imply that the machine has changed, i.e. from 5 to 7 s the machine is already partially demagnetized. This is an important result because it also implies that the proportional-integral (PI) controller for each current is compensating for the demagnetized rotor.

In Fig. 20 the comparison of the DQ currents at their respective references is presented. Notice in Fig. 20b that the speed controller output, namely the Q current reference,

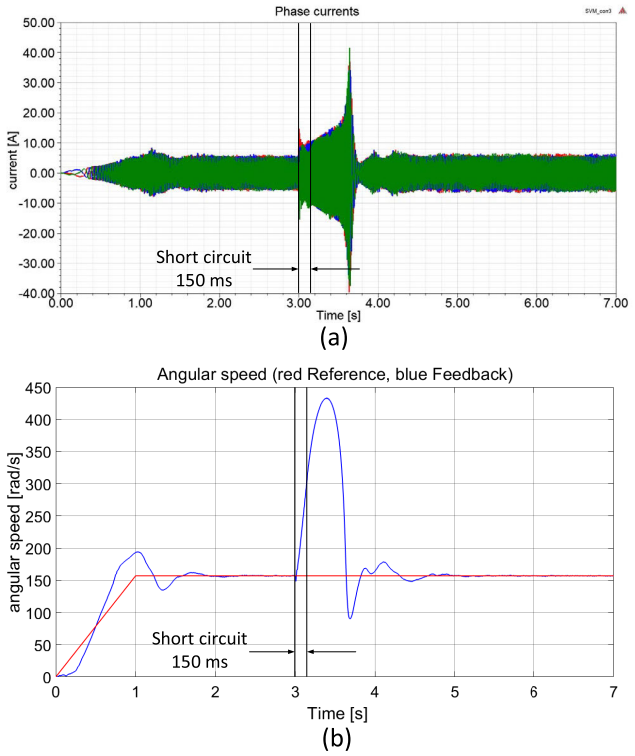

FIGURE 17. Phase currents (a), angular speed (b) during the experiment.

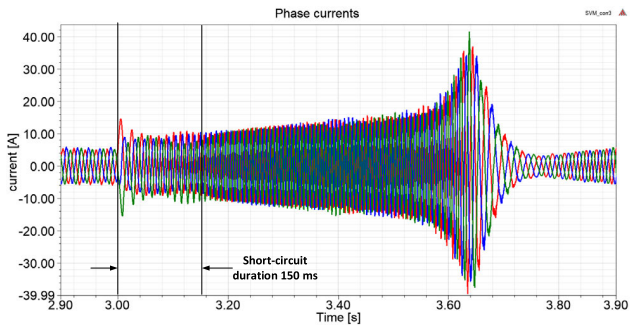

FIGURE 18. Phase currents close-up during fault and after fault clearance.

is limited to ±12. The fact that the speed PI controller is over its limit and that the current PI controllers have also reached their limits (see Fig. 19b), means that the machine is in an uncontrolled state until about 3.65 s when the PMSG suddenly decelerates and the controller brings the machine back to reference speed.

In Fig. 21 the power output of the system and the DC bus voltage are presented. Notice again that although the input power (torque and speed) are the same before and after the fault, there is a difference in the output power after the fault indicating that the machine has lost efficiency. In Fig. 2b is shown that the DC bus voltage never reaches the 1.2 kV limit.

The peak power in Fig. 21a is momentary and is the result of the breaking torque that the system provokes to decelerate the PMSG, i.e. the load acts as a ''breaking resistor''.

In Fig. 22 a second experiment with a shorter short-circuit duration time (100 ms) is presented.

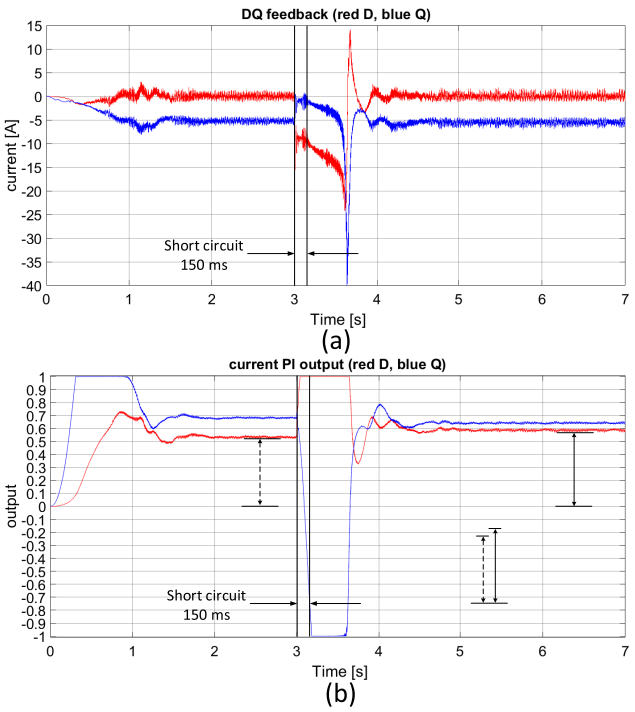

FIGURE 19. DQ current feedback (a) current controller DQ output (b).

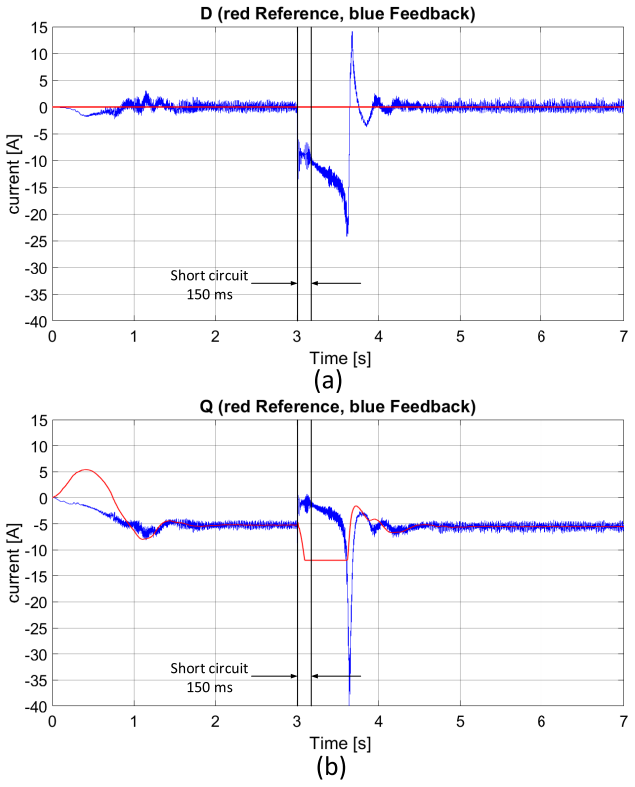

FIGURE 20. D current (a) Q current (b) feedback and reference.

The behavior of the system with a shorter short-circuit is very similar to the previous one. Once again, the short-circuit currents are higher than nominal but the highest currents

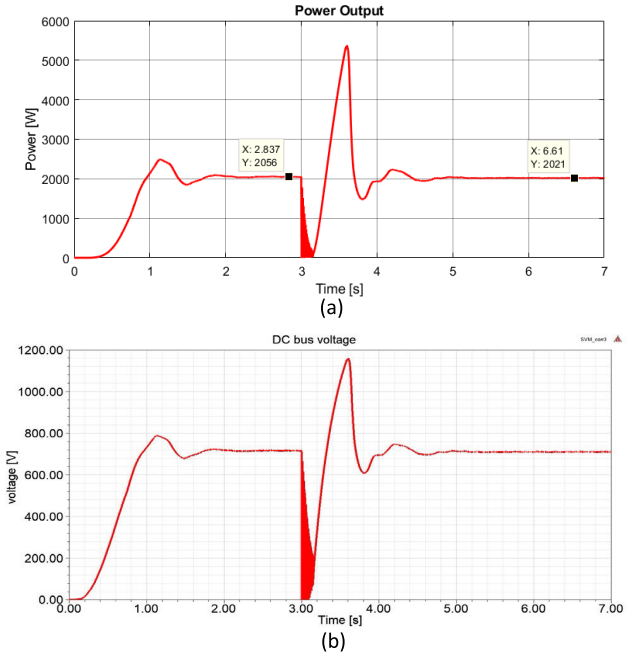

FIGURE 21. Power output at load (a) and DC bus voltage (b).

occur after the short-circuit clearance. This is clearly visible in Fig. 23 where the line-to-line short-circuit occurs at 3 s and is cleared at 3.1 s.

C. DISCUSION OF THE RESULTS

The results show a clear effect of the FOC over the PMSG after the fault clearance. During the short-circuit, and because the input torque from the prime mover stays constant, the PMSG accelerates at a rate dependent, among other factors, on the moment of inertia of the system, 0.009 kg $\cdot$ m^2 for this system. This means that the prime mover produces an acceleration which only ceases until the short circuit is cleared and the control signals return to values within their limits. Here is important to mention that all PI controllers have clamping anti-windup method. This acceleration is well known in hydrogenerators and is limited by the so called ''runaway speed'', or maximum speed the generator can mechanically survive. This can be as high as 3 times the nominal speed [28]. The PMSG rotor was designed with mechanical FEA to withstand 377 rad/s (3600 rpm) within the safety factor limits, as published in [24]. Also, is important to mention that this high speed is very brief, less than 500 ms.

Another important consideration is the DC bus voltage which does not reach 1.2 kV i.e. the limit voltage the IGBTs can withstand. The authors are fully aware of the feasibility that such line-to-line fault in a real system would trigger some protection of the VSC that would shut down the electrical system, at any rate, the main purpose of the experiment was achieved: to study the demagnetization of the PMSG.

From the demagnetization point of view, Fig. 19b and Fig. 21a corroborate that the machine has been partially demagnetized. The D output of the current controller shows a

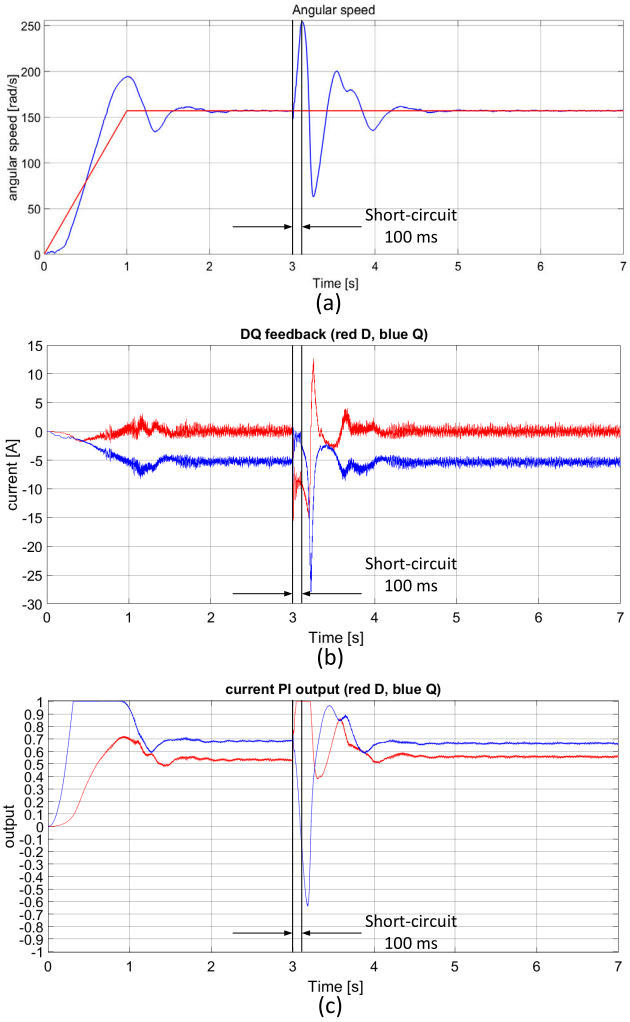

FIGURE 22. Shorter 100 ms short-circuit results, angular speed (a) DQ currents (b), and current PI controller output (c).

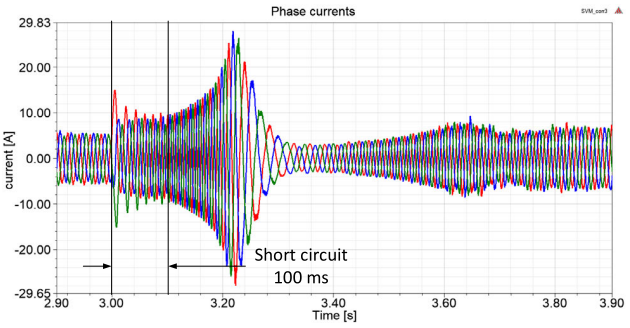

FIGURE 23. Phase currents close-up before, during, and after the 100 ms short-circuit.

higher value after the demagnetization. This coincides with previous results in the literature, e.g. [29], which explain that a partially demagnetized machine needs a bigger D current to compensate for the field lost by the magnets. Also, literature [30] shows a change in the machine efficiency after partial demagnetization. This is visible in Fig. 21a where the output power after demagnetization is 35 W lower than before, i.e. it lost around 1.5 % in efficiency.

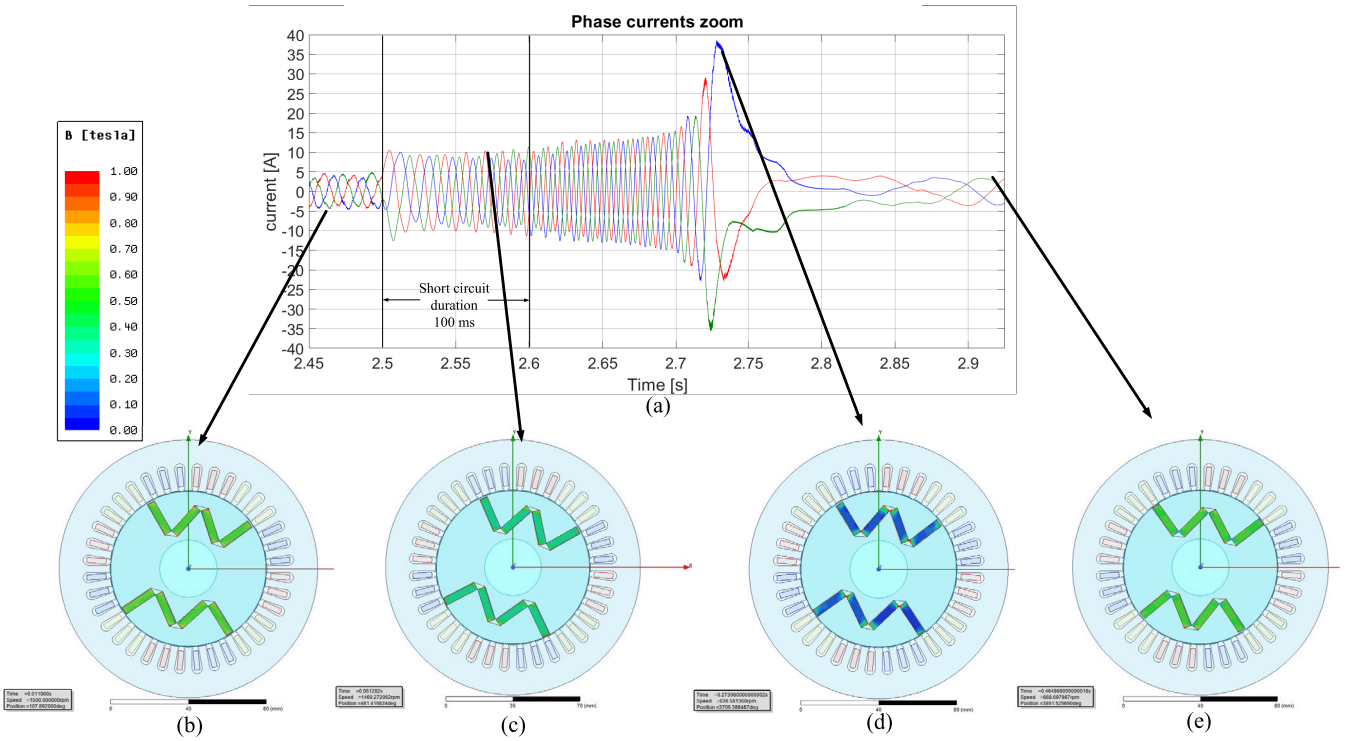

FIGURE 24. Cosimulation results for 2 phase short circuit 80°C magnets and 12 Nm input torque, currents (a), magnets initial magnetic flux density B before the fault (b), during the short circuit (c), in the current peak (d), and after the peak (e).

Finally, Fig. 24 shows the effect of the currents in the rotor permanent magnets before, during and after demagnetization. These results also corroborate that the currents calculated by the cosimulation in these experiments were high enough to bring the N38SH magnets to a partial demagnetization even when the operating temperature was far from the 150 °C rating of the SH classification. As mentioned before, the magnets were assumed to have a constant temperature throughout the experiment (e.g. 80 °C in Fig. 24). This means that the demagnetization mechanism was connected with the armature reaction rather than the temperature change in the magnets, which is assumed to take a longer period of time than the experiments. Note that 80 °C and 100 °C magnets in such a machine, operating continuously in a hot ambient temperature (∼40 °C) is a very plausible temperature for the rotor magnets as shown in [31] where the magnets reached almost 70 °C at an 25 °C ambient temperature.

V. CONCLUSION

Three main contributions can be highlighted from this work. First, the use of a novel tool named cosimulation to model with higher precision the electrical machine and its interaction with a widely used two level voltage source converter based on IGBTs. This was validated multiple times: in open loop with purely resistive load and in closed loop with a 2-level VSC under FOC at 3 kHz switching frequency. All validations showed very good agreement between cosimulation results and experimental measurements.

Second, the feasibility to analyze a line-to-line short circuit during closed loop operation at nominal speed and constant input torque. As presented, the possibility to replicate the experiments and measurements of the short-circuit in the laboratory setup is almost impossible because the destructive nature of the test. This cosimulation tool allows a very accurate modeling and interaction between specialized software for the different parts of the system. In conjunction, the results obtained by the cosimulation are closer to the physical measurements than many models used in model-based control design as was also published by one of the authors in [27].

Third, the demagnetization due to sudden break or deceleration. As was discussed in the last section, the machine shows a different behavior before and after the short-circuit but as shown in the results, the main contributors to the demagnetization are the decelerating currents that occur after the short-circuit and not the short-circuit currents themselves. This is a very important finding because previous literature always focused on the short-circuit currents as the source of demagnetization. In this work, since the machine is working as a generator and the input torque from the prime mover stays constant, then the effect of the speed control through FOC is creating a higher risk for the machine. This is fundamentally different than a previous work published by one of the authors in [32] where the 3-phase short-circuit was studied without FOC and at constant input speed.

As discussed before, the demagnetization presented here is connected with the magnetic field created by the phase currents and opposing the magnets. This occurs in a very dynamic state i.e. rotational speed. Analyses shown that at shorter short-circuit fault duration the demagnetization is also smaller. Further analyses not presented here had shown that

at longer short-circuit fault duration (>160 ms) the machine accelerates beyond a speed where the FOC is not able to decelerate or break (spins out of control). This is the reason why many generator systems, including wind turbines, incorporate a mechanical braking system in the shaft.

The results presented here will be further analyzed for demagnetization detection through current signal analysis and other methods. This is possible thanks to the accuracy of the cosimulation and its calculations.

REFERENCES

[1] J. M. D. Coey, *Magnetism and Magnetic Materials*. Cambridge, U.K.: Cambridge Univ. Press, 2010.

[2] O. Gutfleisch, M. A. Willard, E. Brück, C. H. Chen, S. G. Sankar, and J. P. Liu, "Magnetic materials and devices for the 21st century: Stronger, lighter, and more energy efficient," *Adv. Mater.*, vol. 23, no. 7, pp. 821–842, Feb. 2011.

[3] G.-H. Kang, J.-P. Hong, G.-T. Kim, and J.-W. Park, "Improved parameter modeling of interior permanent magnet synchronous motor based on finite element analysis," *IEEE Trans. Magn.*, vol. 36, no. 4, pp. 1867–1870, Jul. 2000.

[4] G.-H. Kang, J. Hur, H. Nam, J.-P. Hong, and G.-T. Kim, "Analysis of irreversible magnet demagnetization in line-start motors based on the finite-element method," *IEEE Trans. Magn.*, vol. 39, no. 3, pp. 1488–1491, May 2003.

[5] S. Ruoho, E. Dlala, and A. Arkkio, "Comparison of demagnetization models for finite-element analysis of permanent-magnet synchronous machines," *IEEE Trans. Magn.*, vol. 43, no. 11, pp. 3964–3968, Nov. 2007.

[6] S. Ruoho, J. Kolehmainen, J. Ikaheimo, and A. Arkkio, "Interdependence of demagnetization, loading, and temperature rise in a permanent-magnet synchronous motor," *IEEE Trans. Magn.*, vol. 46, no. 3, pp. 949–953, Mar. 2010.

[7] W. N. Fu and S. L. Ho, "Dynamic demagnetization computation of permanent magnet motors using finite element method with normal magnetization curves," *IEEE Trans. Appl. Supercond.*, vol. 20, no. 3, pp. 851–855, Jun. 2010.

[8] P. Zhou, D. Lin, Y. Xiao, N. Lambert, and M. A. Rahman, "Temperature-dependent demagnetization model of permanent magnets for finite element analysis," *IEEE Trans. Magn.*, vol. 48, no. 2, pp. 1031–1034, Feb. 2012.

[9] P. Zhou, D. Lin, W. N. Fu, B. Ionescu, and Z. J. Cendes, "A general cosimulation approach for coupled field-circuit problems," *IEEE Trans. Magn.*, vol. 42, no. 4, pp. 1051–1054, Apr. 2006.

[10] K.-C. Kim, K. Kim, H. J. Kim, and J. Lee, "Demagnetization analysis of permanent magnets according to rotor types of interior permanent magnet synchronous motor," *IEEE Trans. Magn.*, vol. 45, no. 6, pp. 2799–2802, Jun. 2009.

[11] C. Kral, R. Sprangers, J. Waarma, A. Haumer, O. Winter, and E. Lomonova, "Modeling demagnetization effects in permanent magnet synchronous machines," in *Proc. 19th Int. Conf. Electr. Mach. (ICEM)*, Sep. 2010, pp. 1–6.

[12] R. Fratila, A. Benabou, A. Tounzi, and J. C. Mipo, "Nonlinear modeling of magnetization loss in permanent magnets," *IEEE Trans. Magn.*, vol. 48, no. 11, pp. 2957–2960, Nov. 2012.

[13] S. Sjokvist and S. Eriksson, "Experimental verification of a simulation model for partial demagnetization of permanent magnets," *IEEE Trans. Magn.*, vol. 50, no. 12, pp. 1–5, Dec. 2014.

[14] P. Peng, J. Zhang, W. Li, F. Leonardi, C. Rong, M. W. Degner, F. Liang, and L. Zhu, "Temperature-dependent demagnetization of Nd-Fe-B magnets for electrified vehicles," in *Proc. IEEE Int. Electr. Mach. Drives Conf. (IEMDC)*, May 2019, pp. 2056–2062.

[15] K.-T. Kim, Y.-S. Lee, and J. Hur, "Transient analysis of irreversible demagnetization of permanent-magnet brushless DC motor with interturn fault under the operating state," *IEEE Trans. Ind. Appl.*, vol. 50, no. 5, pp. 3357–3364, Sep. 2014.

[16] H.-K. Kim and J. Hur, "Dynamic characteristic analysis of irreversible demagnetization in SPM- and IPM-type BLDC motors," *IEEE Trans. Ind. Appl.*, vol. 53, no. 2, pp. 982–990, Mar. 2017.

[17] G. Choi and T. M. Jahns, "Demagnetization characteristics of permanent magnet synchronous machines," in *Proc. 40th Annu. Conf. IEEE Ind. Electron. Soc. (IECON)*, Oct. 2014, pp. 469–475.

[18] G. Choi, Y. Zhang, and T. M. Jahns, "Experimental verification of rotor demagnetization in a fractional-slot concentrated-winding PM synchronous machine under drive fault conditions," *IEEE Trans. Ind. Appl.*, vol. 53, no. 4, pp. 3467–3475, Jul. 2017.

[19] B. A. Welchko, T. M. Jahns, W. L. Soong, and J. M. Nagashima, "IPM synchronous machine drive response to symmetrical and asymmetrical short circuit faults," *IEEE Trans. Energy Convers.*, vol. 18, no. 2, pp. 291–298, Jun. 2003.

[20] G. Choi and T. M. Jahns, "Interior permanent magnet synchronous machine rotor demagnetization characteristics under fault conditions," in *Proc. IEEE Energy Convers. Congr. Expo.*, Sep. 2013, pp. 2500–2507.

[21] G. Choi and T. M. Jahns, "PM synchronous machine drive response to asymmetrical short-circuit faults," in *Proc. IEEE Energy Convers. Congr. Expo. (ECCE)*, Sep. 2014, pp. 622–629.

[22] J. A. Tapia, F. Leonardi, and T. A. Lipo, "Consequent-pole permanent-magnet machine with extended field-weakening capability," *IEEE Trans. Ind. Appl.*, vol. 39, no. 6, pp. 1704–1709, Nov. 2003.

[23] R. T. Ugale, B. N. Chaudhari, S. Baka, S. S. Dambhare, and A. Pramanik, "Induced pole rotor structure for line start permanent magnet synchronous motors," *IET Electr. Power Appl.*, vol. 8, no. 4, pp. 131–140, Apr. 2014.

[24] R. E. Quintal-Palomo, M. Gwozdziewicz, and M. Dybkowski, "Design and test of an internal permanent magnet generator for small wind turbine applications," in *Proc. 19th Eur. Conf. Power Electron. Appl. (EPE ECCE Eur.)*, Sep. 2017, pp. P.1–P.4.

[25] C. Indukta. Sh 90L4. (2019). *Sh90-L4 Electrical Parameters*. Accessed: Mar. 11, 2019. [Online]. Available: https://www.cantonigroup.com/celma/en/page/offer/details/1/146/Sh90L-4

[26] Supermagnete. (2020). *What Temperatures Can Magnets Withstand?* Frequently Asked Questions. [Online]. Available: https://www.supermagnete.de/eng/faq/What-temperatures-can-magnets-sustain

[27] R. E. Quintal-Palomo, M. Gwozdziewicz, and M. Dybkowski, "Modelling and co-simulation of a permanent magnet synchronous generator," *COMPEL-Int. J. Comput. Math. Electr. Electron. Eng.*, vol. 38, no. 6, pp. 1904–1917, Jul. 2019.

[28] D. J. Littler, *Turbines, Generators and Associated Plant*, 3rd ed. Oxford, U.K.: Pergamon Press, 1991.

[29] Z. Ullah and J. Hur, "A comprehensive review of winding short circuit fault and irreversible demagnetization fault detection in PM type machines," *Energies*, vol. 11, no. 12, p. 3309, Nov. 2018.

[30] D. Fernandez, M. Martinez, D. Reigosa, J. M. Guerrero, C. M. S. Alvarez, and F. Briz, "Impact of machine magnetization state on permanent magnet losses in permanent magnet synchronous machines," *IEEE Trans. Ind. Appl.*, vol. 55, no. 1, pp. 344–353, Jan. 2019.

[31] D. D. Reigosa, D. Fernandez, H. Yoshida, T. Kato, and F. Briz, "Permanent-magnet temperature estimation in PMSMs using pulsating high-frequency current injection," *IEEE Trans. Ind. Appl.*, vol. 51, no. 4, pp. 3159–3168, Jul. 2015.

[32] R. E. Q. Palomo and M. Gwozdziewicz, "Effect of demagnetization on a consequent pole IPM synchronous generator," *Energies*, vol. 13, no. 23, p. 6371, Dec. 2020.

ROBERTO EDUARDO QUINTAL-PALOMO (Member, IEEE) received the B.S. degree in electronics engineering from the Monterrey Institute of Technology (ITESM), Monterrey, Mexico, in 2005, the M.S. degree in power and automation from the University of Duisburg-Essen, Duisburg, Germany, in 2010, and the Ph.D. degree in electrical and electronics automation from the Wrocław University of Science and Technology, Wrocław, Poland, in 2020.

From 2005 to 2006, he was a Laboratory Technician with the Mechatronics Department, Faculty of Engineering, Autonomous University of Yucatan (UADY), where he has been an Associate Professor, since 2010. His research interests include electrical machines, power electronics, and renewable energies. He was a recipient of the Scholarship from the Mexican Council of Science and Technology (CONACYT) and the German Academic Exchange Service (DAAD) from 2007 to 2010, and the Best Presentation Award at the National Conference of Control in Power Electronics and Electric Drives (SENE), Lodz, Poland, in 2019.

MANUEL FLOTA-BAÑUELOS (Member, IEEE) received the B.S. degree in electronics engineering from the Mérida Institute of Technology, Mérida, Mexico, in 1999, and the M.S. and Ph.D. degrees from the Autonomous University of San Luis Potosi, Mexico, in 2005 and 2009, respectively.

He is currently a Professor with the Renewable Energies Department, Faculty of Engineering, Autonomous University of Yucatan (UADY). His research interests include non-linear control, observers, electrical power systems, and efficient use of energy sources.

ALI BASSAM received the Ph.D. degree in energy engineering from the Institute of Renewable Energies, National Autonomous University of Mexico (UNAM), in 2012.

Since 2014, he has been a Professor with the Renewable Energy Department, Faculty of Engineering, Autonomous University of Yucatan (UADY). He is currently a member of the Mexican National System of Researchers and a collaborator of several research projects in Mexico. His research interest includes modeling of energy systems and their optimization using new artificial intelligence techniques.

RICARDO PEÓN-ESCALANTE received the B.S. degree in mechanical engineering from the Mexico University of Technology, in 2002, and the M.S. degree in mechanical engineering from the National Autonomous University of Mexico (UNAM), in 2004.

Since 2005, he has been an Associate Professor with the Mechatronics Department, Faculty of Engineering, Autonomous University of Yucatan (UADY). His main research interest includes the analysis and synthesis of mechanisms.

FRANCISCO PEÑUÑURI received the B.S. degree in physics from University of Sonora, Mexico, in 2001, and the M.S. degree in applied physics and the Ph.D. degree in theoretical physics from the Center for Research and Advanced Studies (CINVESTAV), National Polytechnic Institute, Mexico, in 2004 and 2007, respectively.

Since 2003, he has been with the Physics Department, Faculty of Engineering, Autonomous University of Yucatan. His research interests include analytic mechanics, evolutionary optimization, automatic differentiation, and computational physics.

MATEUSZ DYBKOWSKI received the Ph.D. and D.Sc. degrees from the Wrocław University of Science and Technology, Wrocław, Poland, in 2008 and 2014, respectively. Since 2008, he has been a member of the Academic Staff with the Electrical Drives Control, Institute of Electrical Machines, Drives and Measurements, Wrocław University of Science and Technology, where he has been a Professor, since 2016. His main research interests include the induction motor drive control and state variable estimations, control theory applications in electrical drives, digital signal processors, and field-programmable gate array applications.